Analysis of Wing Leading Edge Data

Upender K. Kaul
Intelligent Systems Division
NASA Ames Research Center
Moffett Field, CA 94035

Abstract

Some selected segments of the STS114 ascent and on-orbit data as well as some selected laboratory test article data have been analyzed using wavelets, power spectrum and autocorrelation functions. Additionally, a noise test was performed on these data segments to confirm the presence or absence of white noise behavior in the data. This study was initially directed at characterizing the on-orbit background data against which an impact signature during on-orbit operation could be identified. The laboratory data analyzed here correspond to some impact signatures that mimic types of impacts to the orbiter that it may be subjected to during ascent. A simple hypervelocity impact to an RCC airfoil typical of on-orbit operation was modeled using the finite difference structural dynamic simulator, FiDDLE[1]. Another lower velocity impact typical of ascent conditions was also modeled. Even though there are differences between the actual wing leading edge and the simple airfoil geometries, a comparison between some ascent phase signatures and this modeled signature has provided useful insights. Indeed, the high frequency signatures in the range of 4 - 5 Khz that are observed in the modeling results is also seen embedded in these ascent data, thus leading to a strong possibility that the orbiter was subjected to some form of high velocity impact(s) during this ascent phase. The hypervelocity impact signatures have a very high spectral content present in them. Any high frequency accelerometer signal during on-orbit mode would thus indicate an impact event.

Keywords

Wing Leading Edge Impact Detection System, Accelerometer Data, Ascent Data, On-Orbit Background Characterization, Wavelet, Power Spectrum, Autocorrelation Function, Noise Test, Finite Difference Impact Signature Modeling, Hypervelocity Impact Signature

Introduction

A large amount of accelerometer data has been collected from the STS114 shuttle wing leading edge impact detection system[2]. The data from 66 accelerometers on each wing, with three accelerometers connected to each sensor unit, were collected during the ascent phase and intermittently during the on-orbit phase. Selected data from a few of these units have been analyzed in this short note to help characterize a segment of the on-orbit background. Also, data from some “quiescent” segments as well as max Q segment in the ascent phase have been analyzed. From the few selected segments of the data analyzed, it appears that there are some narrow frequency bands present in the “quiescent” phases of ascent, namely, pre-SSME ignition and post-ET separation phases, that stand out against a white noise background. Similarly, there are some high frequency bands around 3.7 Khz and 4.3 Khz embedded in the ascent data around the max Q segment as seen on unit

1023, indicating the presence of possible impacts. This is supported by modeling results corresponding to a high velocity impact on an airfoil. The finite difference model predicts impact signatures with a spectral content of a few Khz to a few hundred Khz, depending on the location of the numerical sensor and the measurement quantity.

Three standard techniques of analyzing the data have been used in the present study: wavelets, autocorrelation function and the power spectrum. Additionally, another commonly used technique, albeit approximate, has been used to confirm the presence or absence of white noise background in a given data set. All these techniques are established in the literature and they will not be delved into here. Only, the analysis results will be reported here.

Results

All the WLEIDS data analysis results were obtained in Matlab[3]. Modeling and analysis results were obtained using the methodology reported earlier[1,4,5,6]. Modeling results correspond to an airfoil geometry with material properties as those of the RCC panels used for the orbiter wing leading edge. So, the modeled frequency response of the airfoil can be compared, within reason, to the actual wing leading edge response of the orbiter, since the material properties of the structure play a predominant role in defining the local frequency response. There are differences though, but a qualitative comparison between the WLEIDS data and the modeled data reveals that the presence of a high frequency spectral content in ascent data on a particular unit, 1023, during the high Q phase, may be due to an impact. This is a useful finding and lends support for further finite difference modeling efforts in this area.

We shall discuss the modeling results first. The airfoil cross-section is shown in Fig 1(a). Actual test article is shown in Fig 1(b). Initially, the leading edge of the airfoil is subjected to a high velocity impact (maximum velocity of 525 m/sec) whose signature is governed by a Daubechie wavelet with a median frequency of about 250 KHz. Then, the development of the velocities and the stresses is followed in time upto 0.06 second after impact. The development of the horizontal and vertical velocities is followed in time along a "sensor" location that was picked some distance downstream on the upper airfoil surface, as shown, and the signatures were recorded in time at four stations along a line normal to the airfoil boundary.

First, development of stresses in time is shown plotted in Figs. 2 – 4. Figs. 2(a-c) shows the normal stress at the four "radial" stations along the line AB. Since the outer and inner airfoil boundaries are considered free boundaries, normal and shear stresses vanish there, as shown in Figs. 2(a-c) and 4(a-c), respectively. Tangential stress development is shown in Figs. 3(a-d). Maximum value of tangential stress is attained on the inner boundary and the minimum on the outer boundary, as shown in Figs. 3. This agrees with the analytical annulus solution. Corresponding shear stress evolution is shown in Figs. 4. The normal stress response occurs at about 240 Khz, which is commensurate with the normal impact velocity spectral content. A reversal of phase is seen in normal stress between two interior locations. The tangential stress response shows a 220 Khz frequency content, and the shear stress shows a 145 Khz spectral content.

The horizontal and vertical velocities along the line AB are shown in Figs. 5 and 6 respectively. The horizontal velocity attenuates to zero faster than the vertical velocity. It is also observed that there is a reversal of phase in the velocities on the two interior stations opposite to that on the leading edge and the airfoil interior, as is expected.

The important observation to be made here is that subsequent to the impact, the structural response of the airfoil at these observation locations, in terms of velocities and stresses shows a high frequency content in the neighborhood of 4 Khz. This is about the same spectral content that we see in the ascent data in the high Q segment on one of the units as we shall see below. Similar structural response would be expected when the orbiter is subjected to a hypervelocity micrometeoroid impact. But, impacts at lower velocities such as experimented with in the laboratory, e.g., RCC9R31(1,2,3) microtau (strain gauge) data, the frequency response of the test article is at around 130 Hz as shown through results for channel 1 in Fig. 7 and Fig. 8. Fig. 7 shows a wavelet plot which shows the impact event occurs at data sample around 4,000 with a frequency content of around 130 Hz. Fig. 8 confirms the presence of this 130 Hz spectral content in the impact signature. This structural response is typical of a low velocity impact on a RCC panel.

Fig. 9 shows such a spectral content, approximately 3.7 Khz and 4.3 Khz, present in the high Q data segment on unit 1023 during ascent. However, during the "quiescent" periods during ascent, i.e., during the pre-SSME ignition (say, 1 – 2 sec. segment) and the post-ET separation (e.g., 540 – 541 sec. and 580 – 581 sec. segments), a dominant spectral content around 600 Hz is observed for unit 1036, channel 1, with channels 2 and 3 following suit at a lower power level, in the pre-SSME ignition segment. Fig. 10(a) shows an autocorrelation function plot that clearly shows the presence of the 600 Hz spectral content more pronounced in channel 1 than in channels 2 and 3. Fig. 10(b) shows the same spectral content on the power spectrum plot. Fig. 10© shows that the channel 1 does not reflect white noise behavior in this "quiescent" pre-SSME ignition segment, and Fig. 10(d) shows the corresponding wavelet plot. White noise is indicated if the slope of the curves in Fig. 10© is equal to –1; a zero slope would indicate Brownian type of noise.

Figs. 11(a) and 11(b) show the corresponding autocorrelation function and power spectrum plots for the post ET separation segment (540 – 541 sec.) with similar spectral content persisting across all the three channels followed by Fig. 11(c) showing the corresponding wavelet plot. Similar results hold for the 580 – 581 sec. segment in the post-ET regime (not shown here). Other than this 600 Hz spectral content, the pre-SSME and post-ET segments considered here can be classified as quiescent periods, as far as unit 1036 is concerned, i.e., these segments reflect white noise.

Analysis of the laboratory data from a RCC panel without the accelerometers attached confirmed this as being of electronic origin, as shown in Figs. 12(a) and 12(b) except a 60 Hz spike that is attributed to an electrical activity such as a switch-on event.

Analysis of some on-orbit data segments such as those from unit 1027 over various 1-second intervals spread over a few days confirmed the on-orbit background as being a white noise background. Similarly, analysis of a 1-second on-orbit data record from unit 1051 shows the presence of white noise background, as also from a 1-second data record from unit 1036. The presence of pure white noise is typically shown in Figs. 13(a) and 13(b) for unit 1027 through autocorrelation function and noise test plot..

Analysis of unit 1022 on-orbit 1-second data segment shows a low frequency 1-2 Hz event against a white noise background, as shown in the power spectrum, Fig. 14(a), and the wavelet plot, Fig. 14(b). This event is attributable to a probable astronaut activity.

Finally, wavelet analysis of a specific data file, RespClass, reveals a strong self-similarity, as shown in

Fig. 15(a). This strong similarity is also supported by the autocorrelation function plot, Fig. 15(b). The presence of self-similarity implies the absence of white noise behavior of the data. This is shown in the noise test plot, Fig. 15(c). The curves in Fig. 15(c) indicate more of a Brownian type of noise rather than white noise.

Concluding Remarks

A limited analysis of selected on-orbit and "quiescent" data segments has revealed a white noise background akin to electronic noise. Various events are easily isolated against such a white noise background through a discernible spectral content through analyses techniques such as wavelets, autocorrelation function and power spectrum. The white noise background is consistently confirmed or ruled out by the noise test. The data analysis techniques presented here has proved to be a useful tool in the suite of Wing Leading Edge Impact Detection System, currently under further development and enhancement at the NASA Johnson Space Center.

Acknowledgements

The author would like to acknowledge Joshua Johnson of JSC who provided the WLEIDS STS114 raw data for analysis. The author would also like to thank the following WLEIDS team members with whom he has collaborated at one or the other time during this study, Dave Iverson of NASA Ames, William Prosser of NASA Langley and, especially, NASA JSC team members, George Studor, Tammy Gafka, Elonsio Rayos, Charles McCann and Joshua Johnson. Also, special thanks go to Elonsio Rayos and Tammy Gafka who actively supported this work. Special thanks go to Serdar Uckun of NASA Ames who made this study possible.

References

1. Kaul, U. K., "FiDDLE: A Computer Code for Finite Difference Development of Linear Elasticity in Generalized Curvilinear Coordinates," NASA/TM-2005-213450, January 2005

2. Kaul, U. K., "New Boundary Constraints for Elliptic Systems Used in Grid Generation Problems, Journal of Computational Physics," Vol. 189,2003, pp 476-492

3. MATLAB Version 7.0.1

4. Kaul, U. K., "Finite Difference Modeling and Simulation of Idealized Gear Vibrations," Proc. 5th International Workshop on Structural Health Monitoring, Stanford, California, September 12 – 14, 2005, pg. 1183

5. Kaul, U. K., "Structural Vibration Signature Modeling," Industry Day, NASA Ames Research Center, 2004

6. Kaul, U. K., "Finite Difference Modeling and Simulation of Reference Vibration Signatures," Internal NASA documents, March 2004

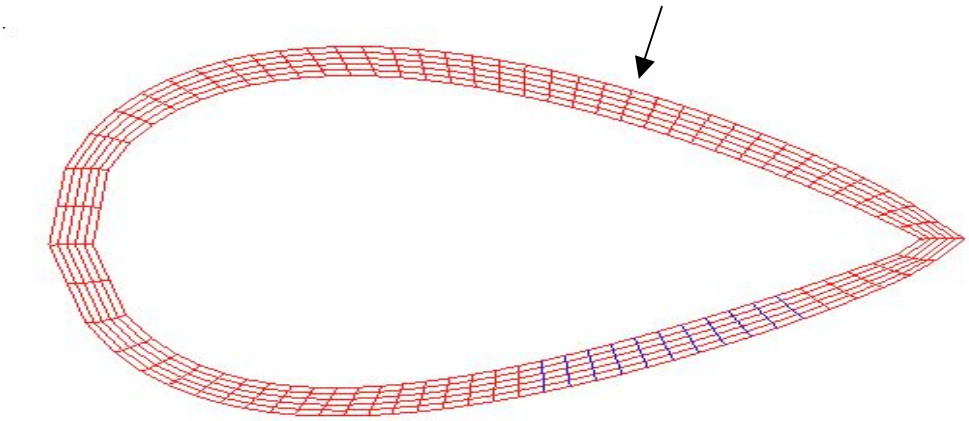

(a). An airfoil geometry

(b). A WLE RCC panel test article

Fig. 1 Geometries for modeling and experiment

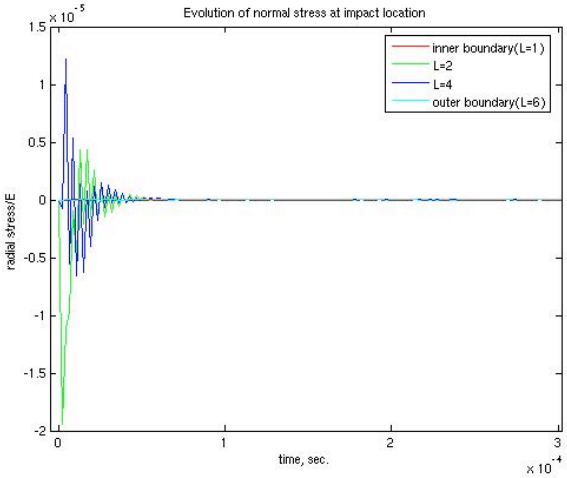

(a)

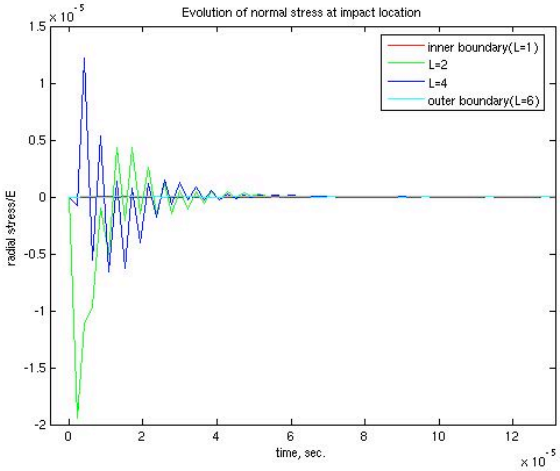

(b) enlarged

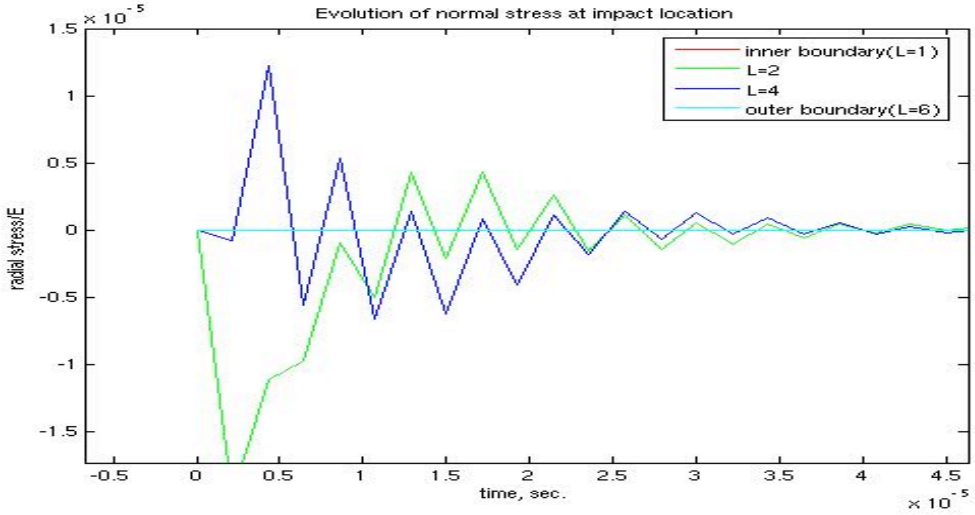

(c) enlarged

Fig. 2 Normal stress time evolution at various stations along the airfoil thickness at the impact location

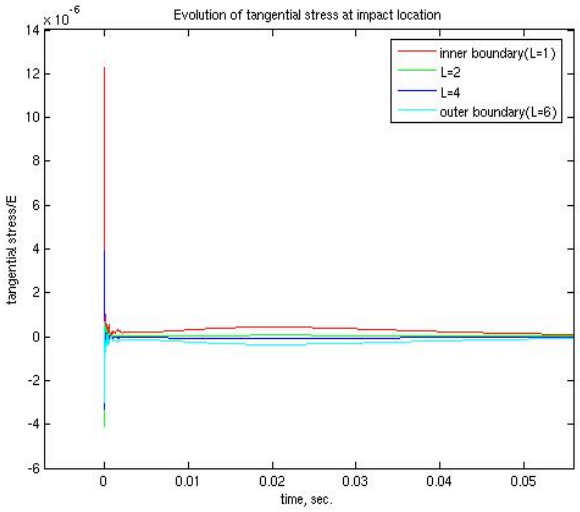

(a)

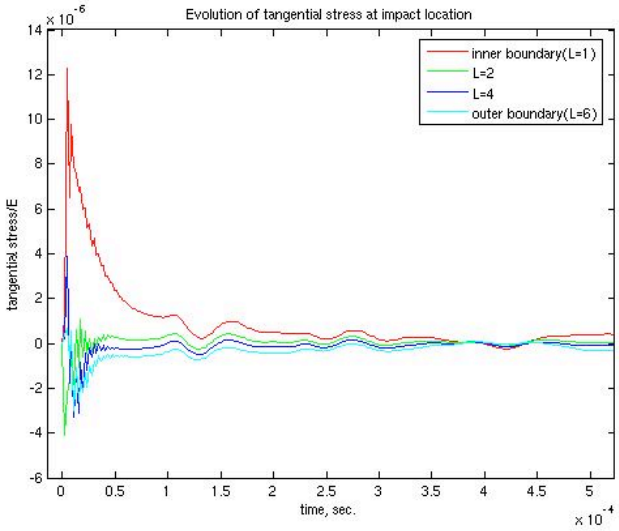

(b) enlarged

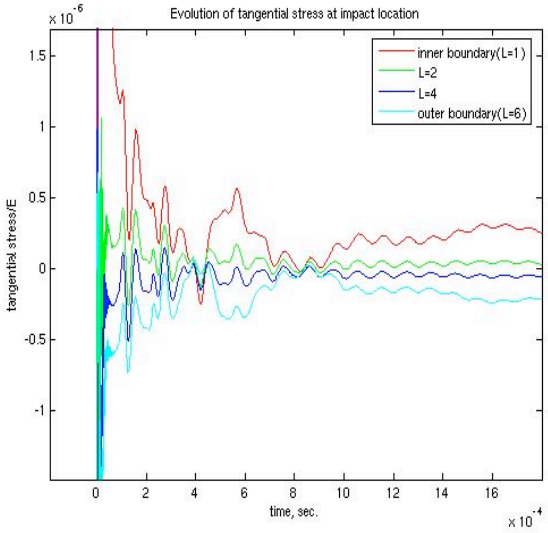

(c) enlarged

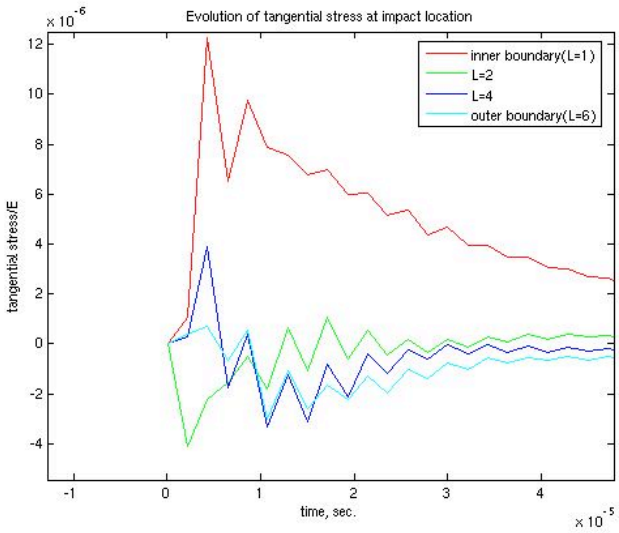

(d) enlarged

Fig. 3 Tangential stress time evolution at various stations along the horizontal line AB between the airfoil leading edge and the interior

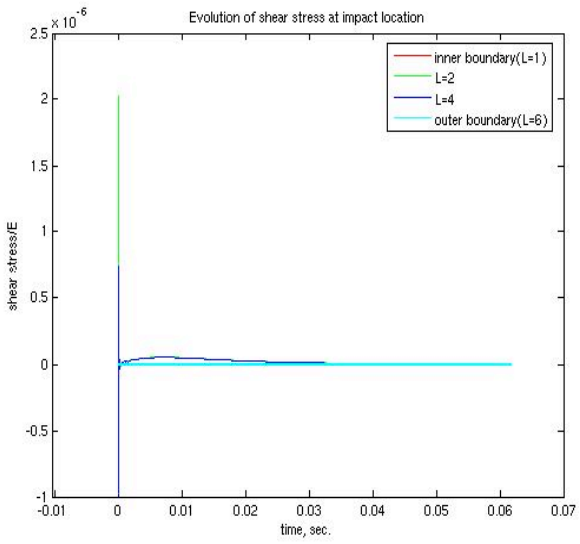

(a)

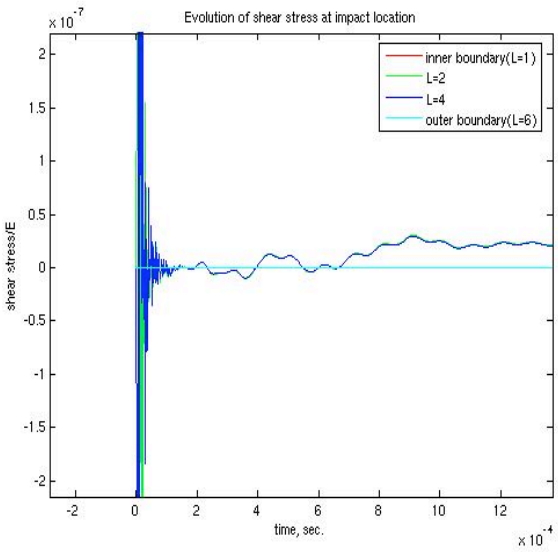

(b) enlarged

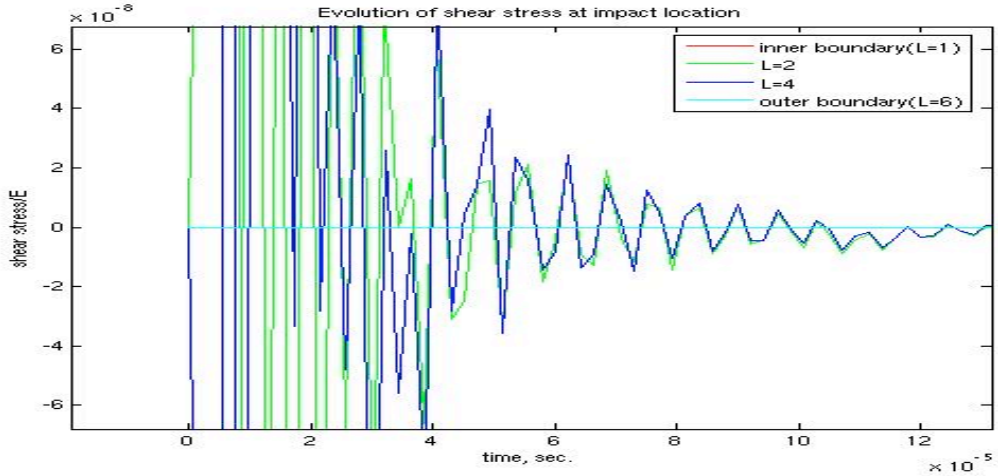

(c) enlarged

Fig. 4 Shear stress time evolution at various stations along the horizontal line AB between the airfoil leading edge and the interior

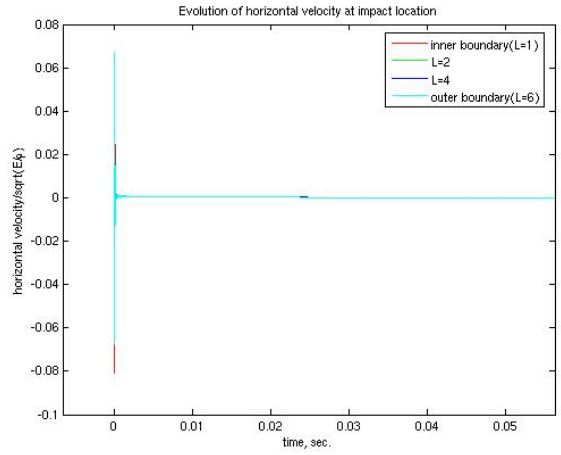

(a)

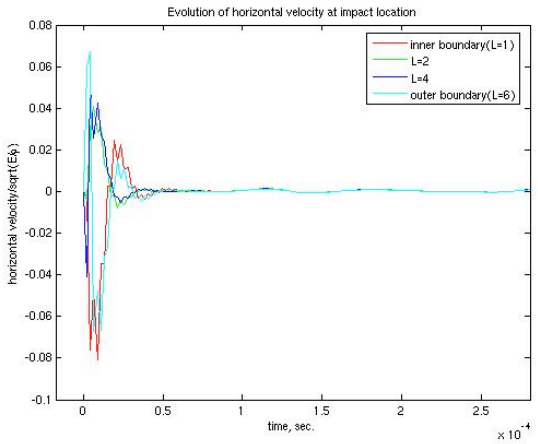

(b) enlarged

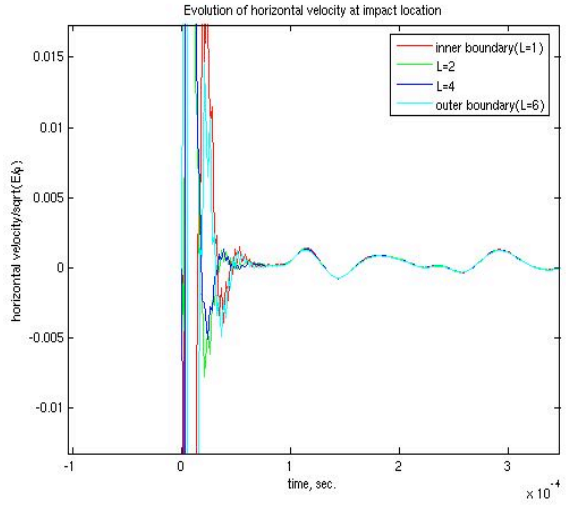

(c) enlarged

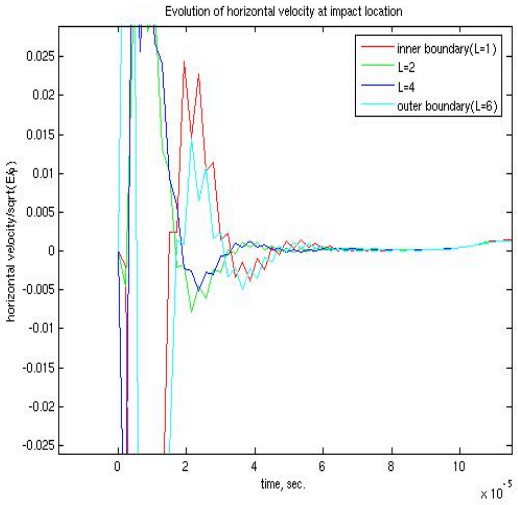

(d) enlarged

Fig. 5 Horizontal velocity time evolution at various stations along the horizontal line AB between the airfoil leading edge and the interior

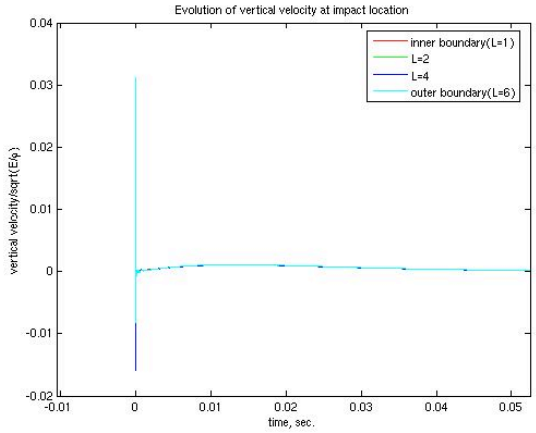

(a)

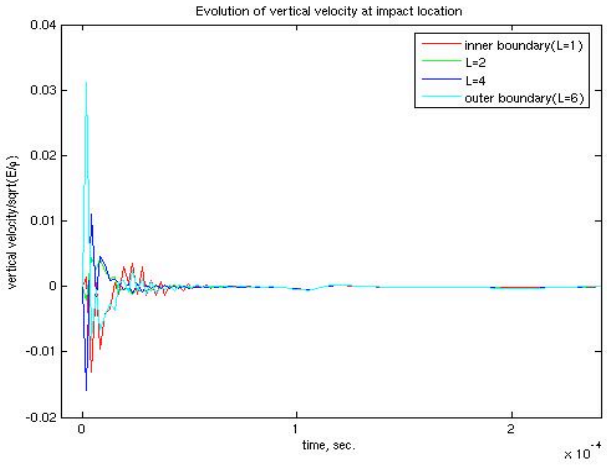

(b) enlarged

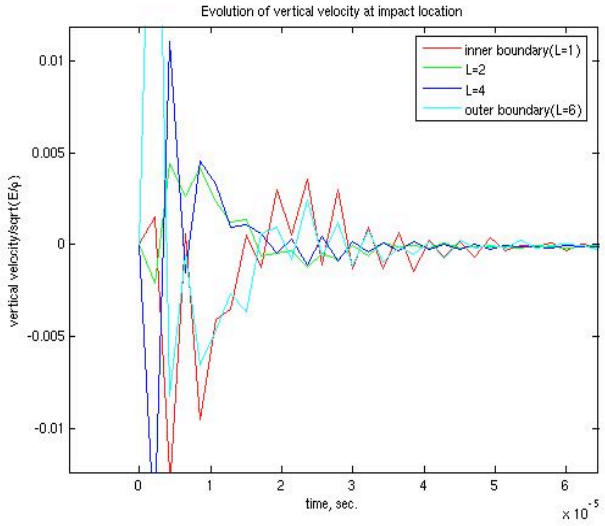

(c) enlarged

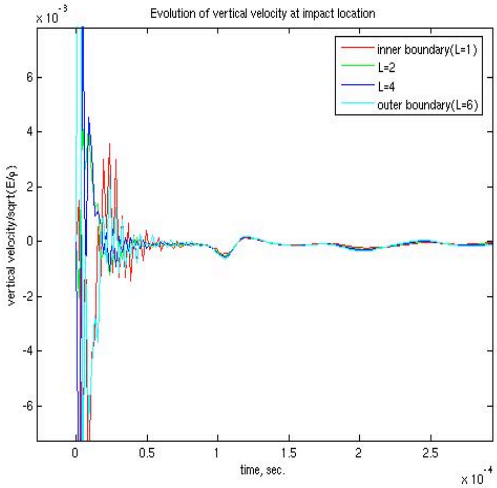

(d) enlarged

Fig. 6 Vertical velocity time evolution at various stations along the horizontal line AB between the airfoil leading edge and the interior

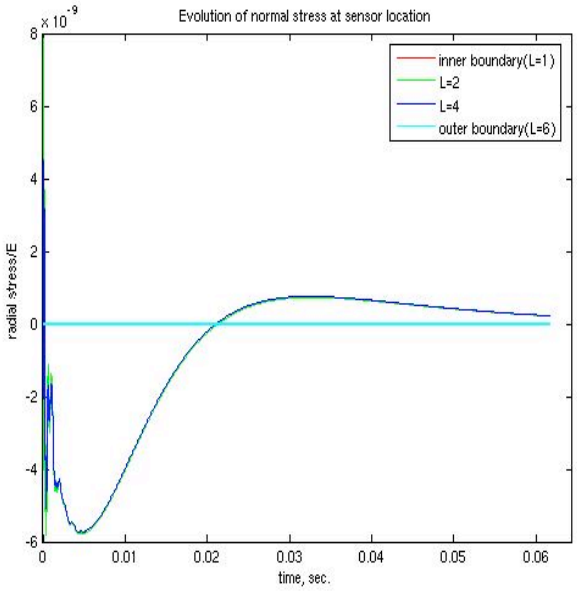

(a)

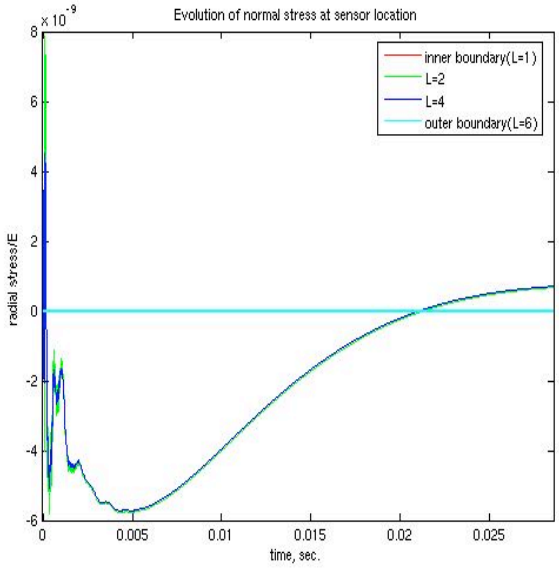

(b) enlarged

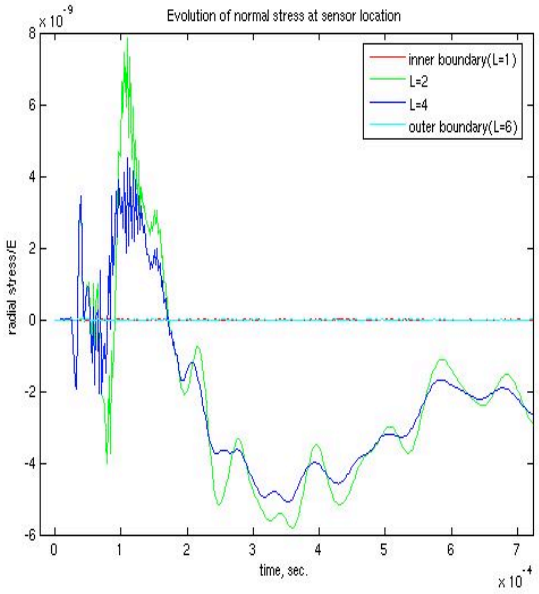

(c) enlarged

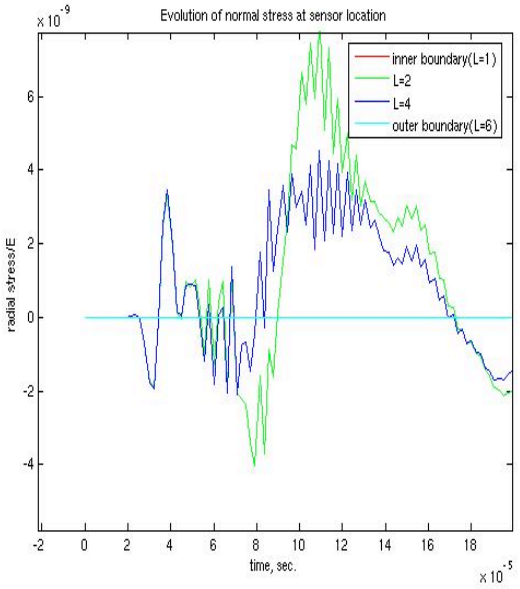

(d) enlarged

Fig. 7 Normal stress time evolution at various stations along the airfoil thickness at the impact location

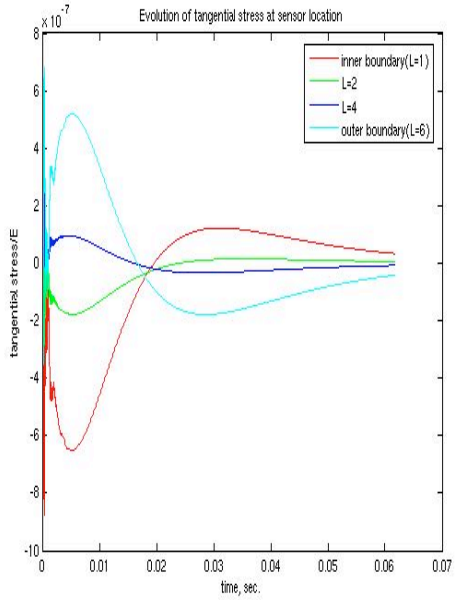

(a)

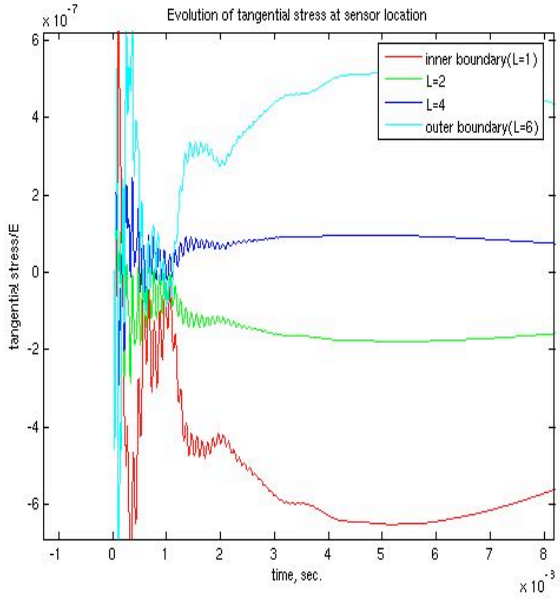

(b) enlarged

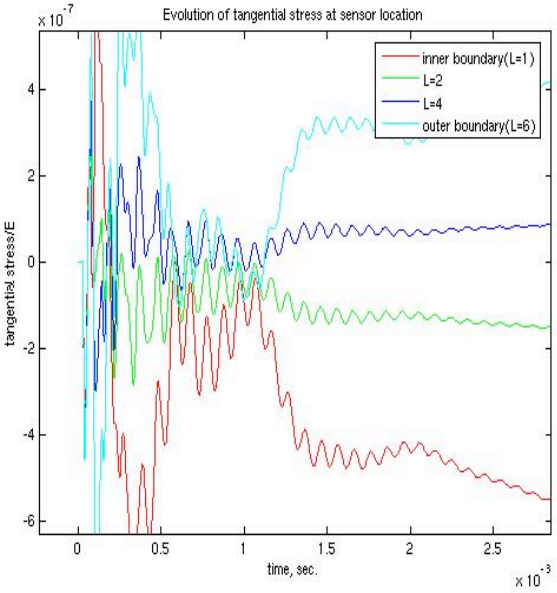

(c) enlarged

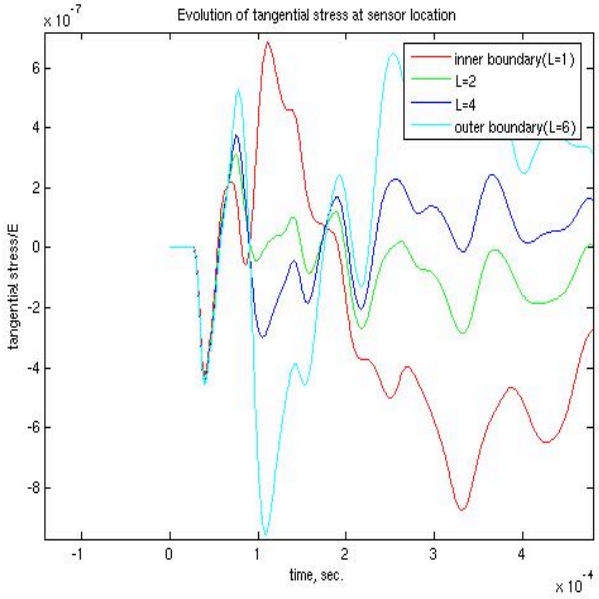

(d) enlarged

Fig. 8 Tangential stress time evolution at various stations along the horizontal line AB between the airfoil leading edge and the interior

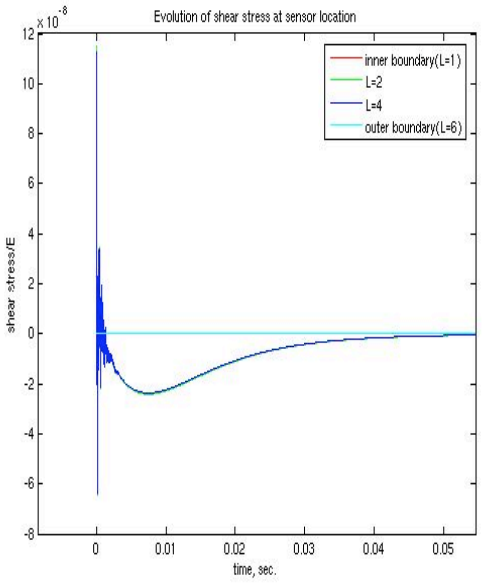

(a)

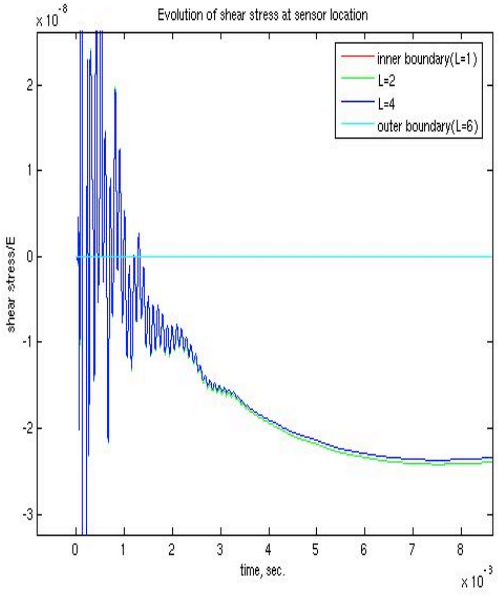

(b) enlarged

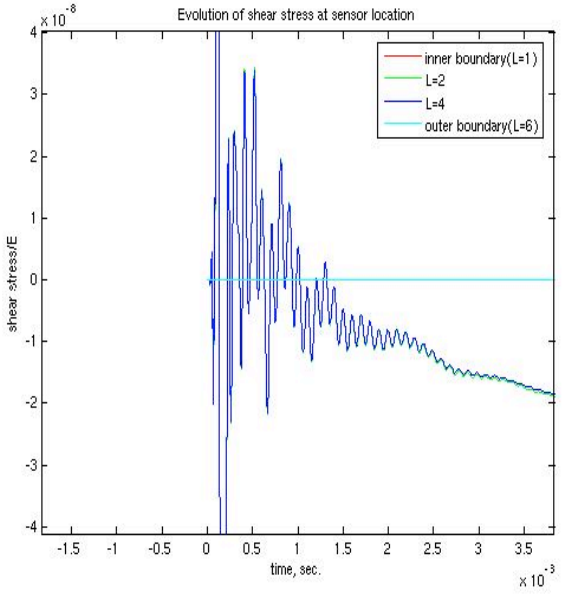

(c) enlarged

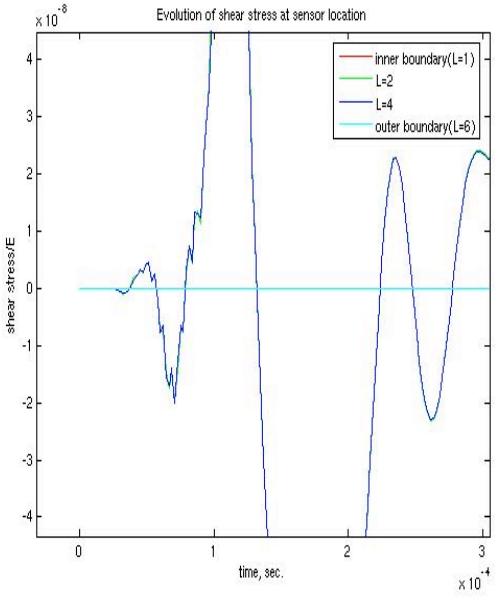

(d) enlarged

Fig. 9 Shear stress time evolution at various stations along the horizontal line AB between the airfoil leading edge and the interior

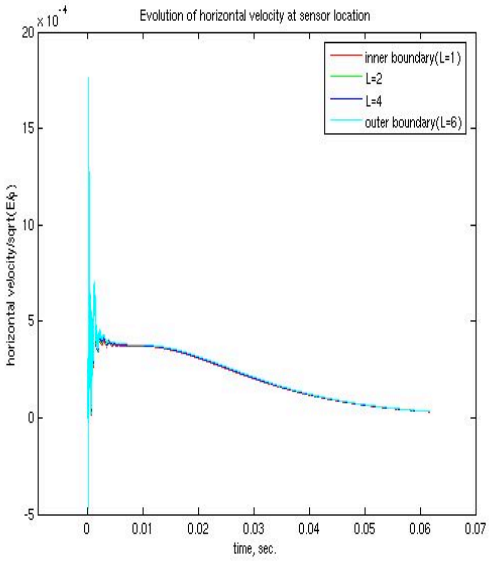

(a)

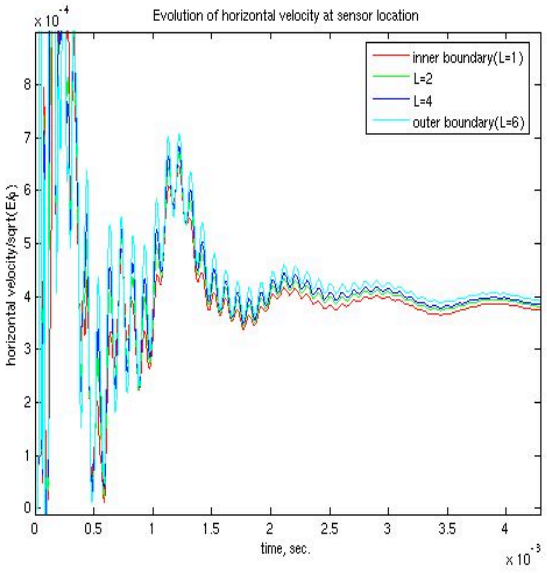

(b) enlarged

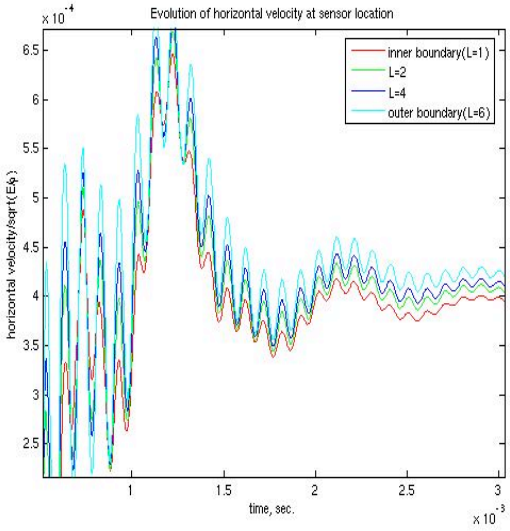

(c) enlarged

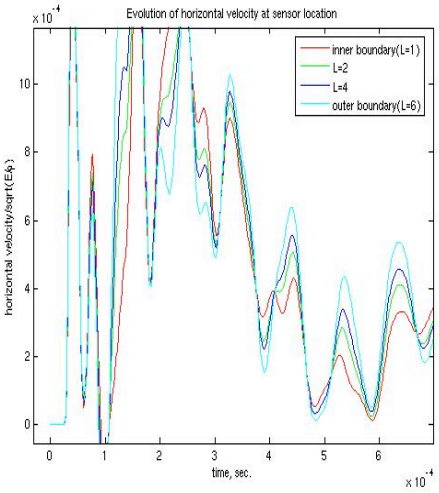

(d) enlarged

Fig. 10 Horizontal velocity time evolution at various stations along the horizontal line AB between the airfoil leading edge and the interior

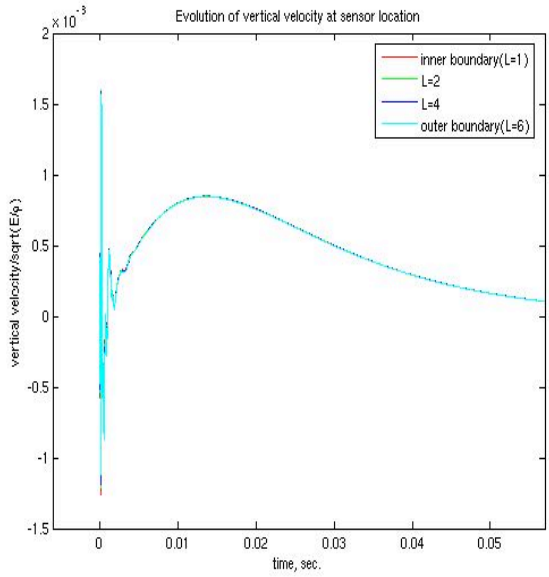

(a)

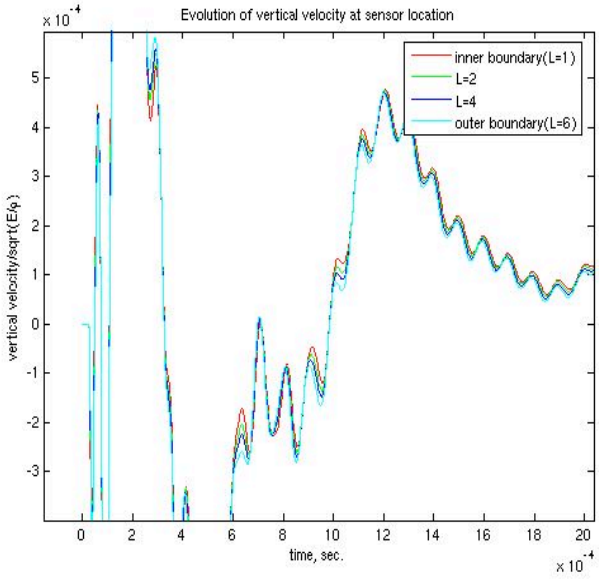

(b) enlarged

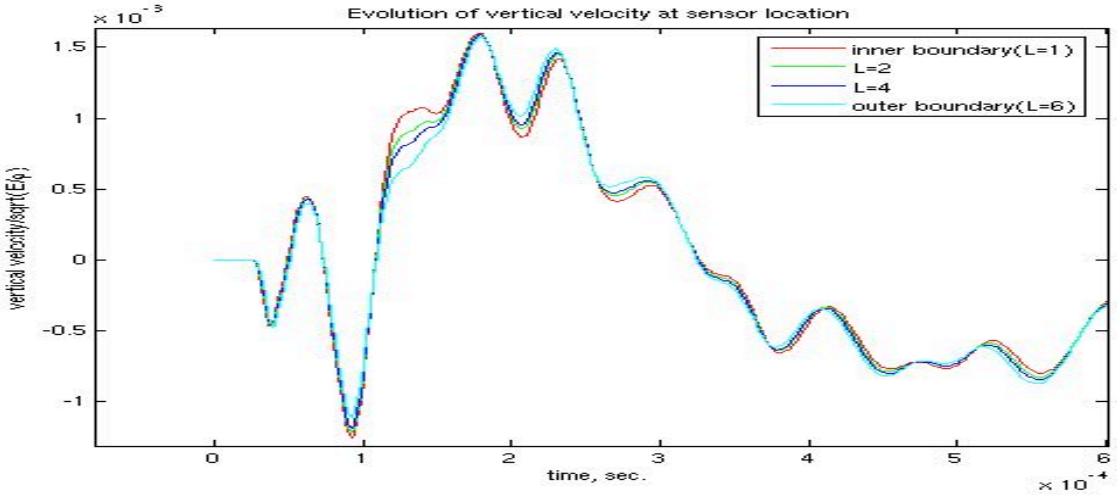

(c) enlarged

Fig. 11 Vertical velocity time evolution at various stations along the horizontal line AB between the airfoil leading edge and the interior

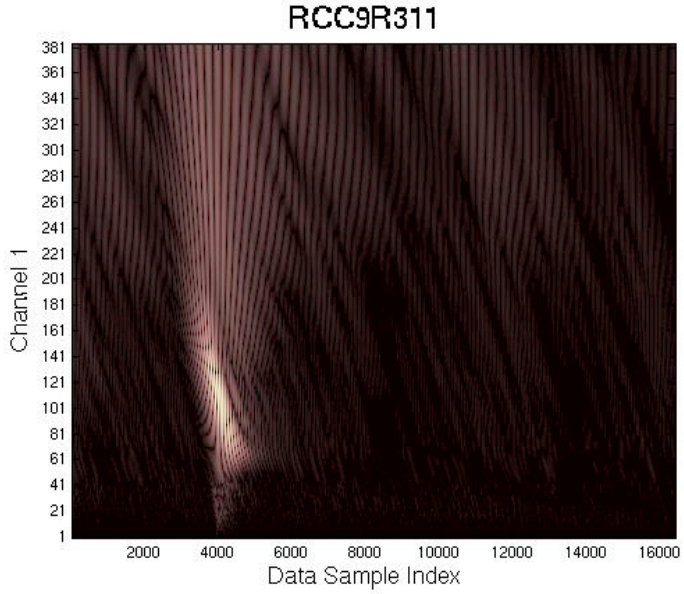

Fig. 7 Wavelet – channel 1: Test article impact response spectral band around 130 Hz

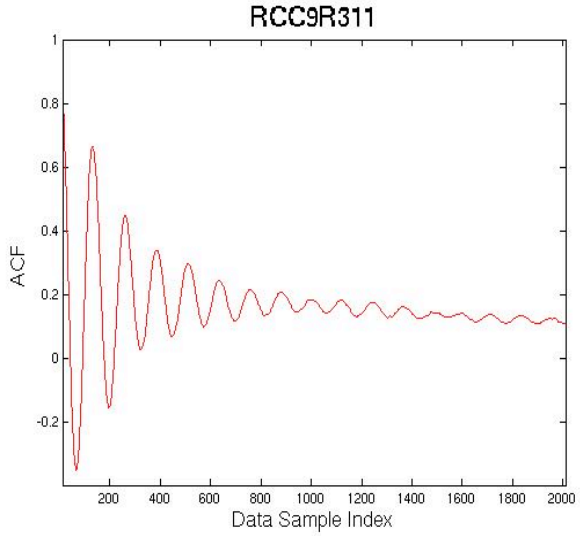

Fig. 8 Autocorrelation function showing 130 Hz spectral content in test article structural response

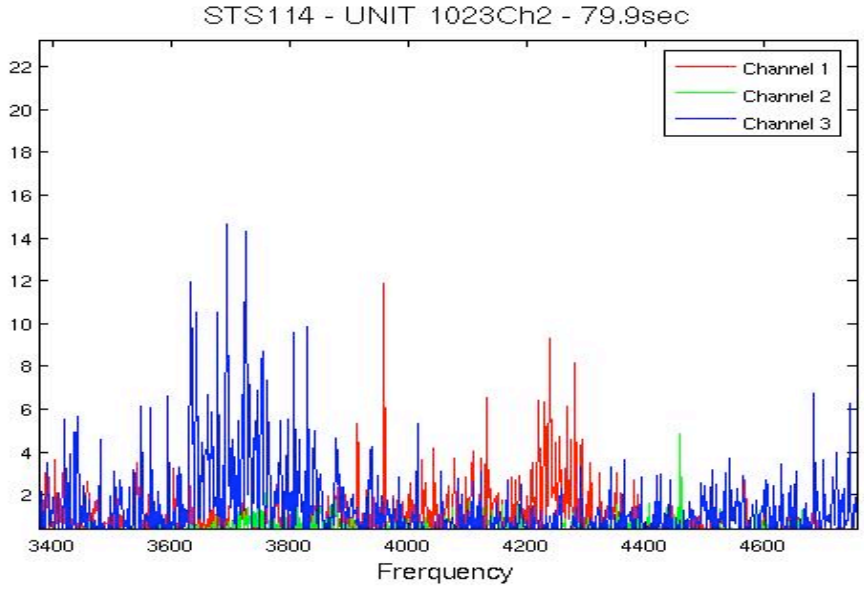

Fig. 9 Spectral content on unit 1023, around 79.9 sec from start of ascent phase

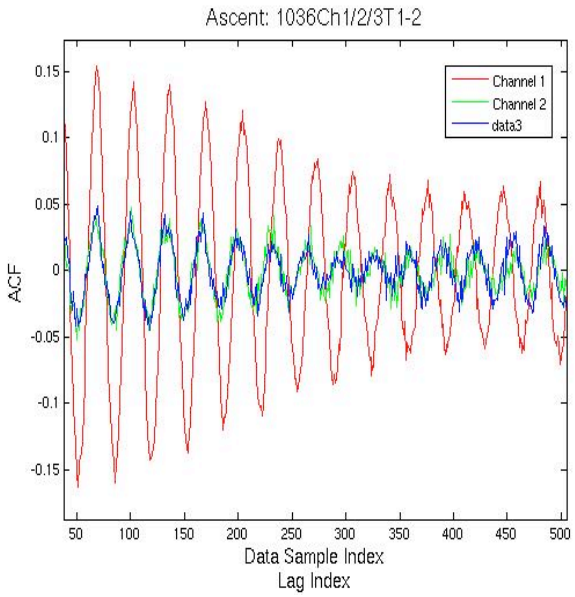

(a) Autocorrelation function

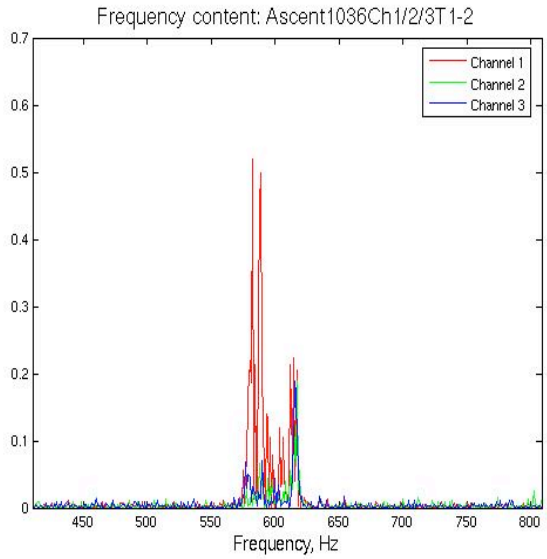

(b) Power spectrum

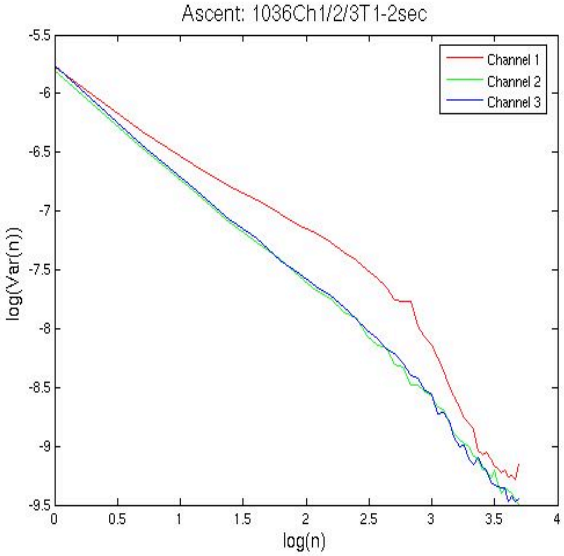

(c) Noise test

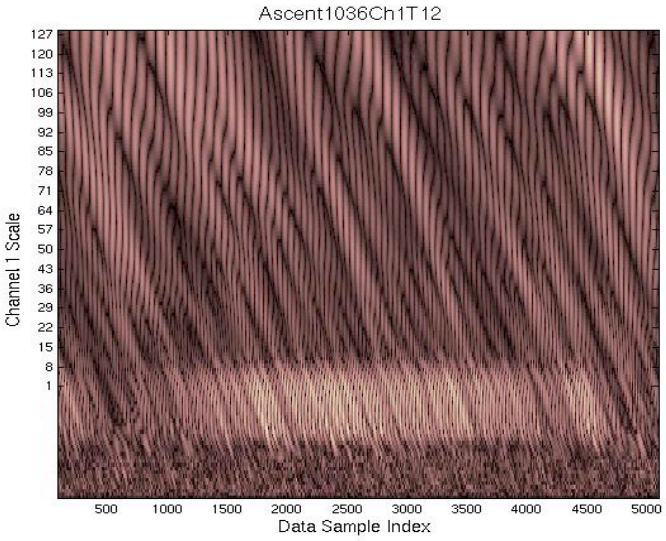

(d) Wavelet – channel 1

Fig. 10 Pre-SSME ignition phase (1 – 2 sec.) shows the presence of spectral band around 600 Hz on unit 1036, dominantly on channel 1

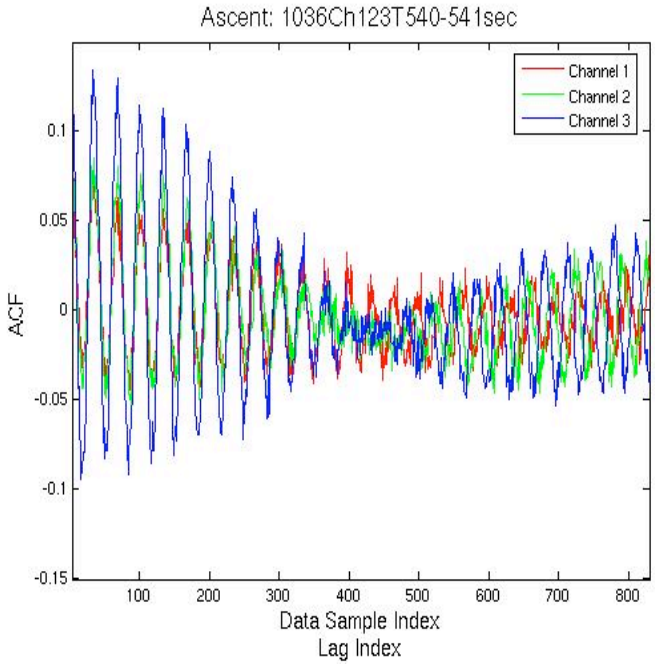

(a) Autocorrelation Function

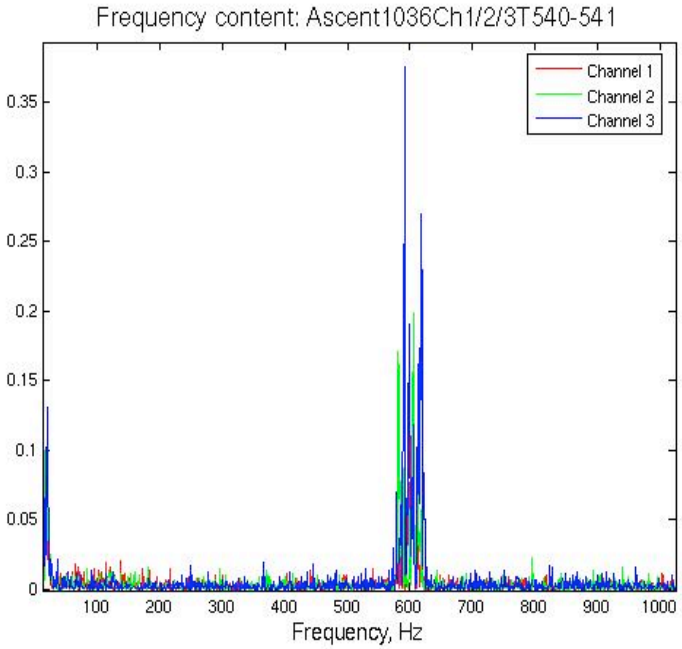

(b) Power spectrum

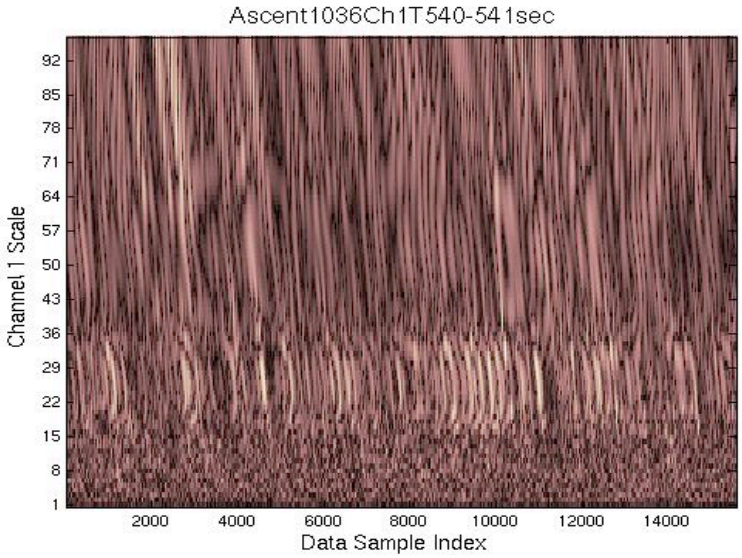

(c) Wavelet – channel 1

Fig. 11 Post-ET separation phase (540 – 541 sec.) shows the presence of spectral band around 600 Hz on unit 1036

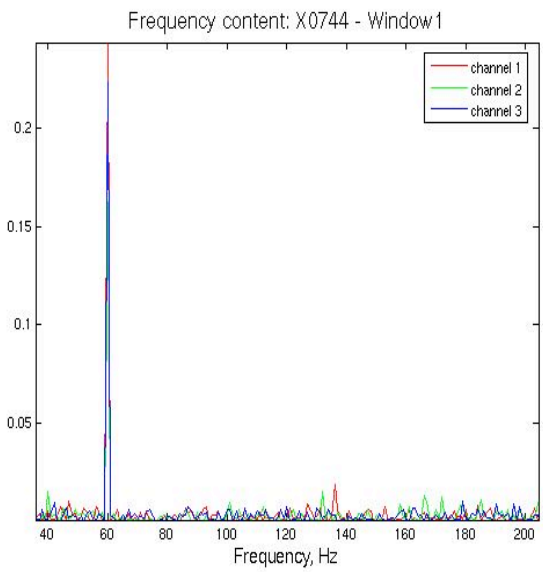

(a) Power spectrum

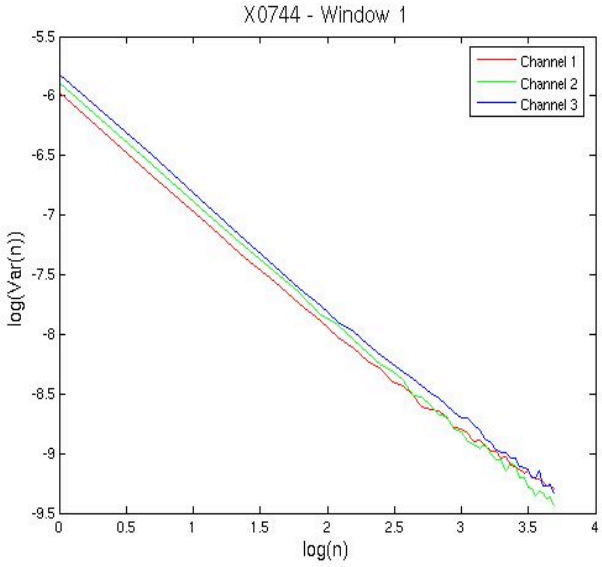

(b) Noise test

Fig. 12 Characterization of background as electrical white noise without accelerometers attached

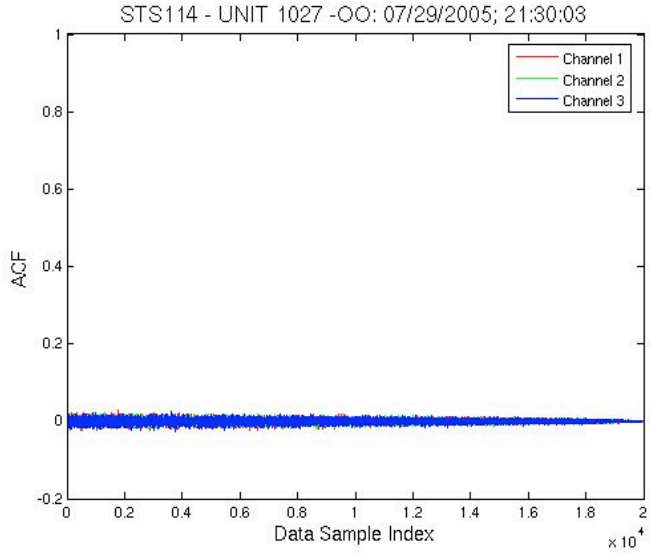

(a) Autocorrelation function

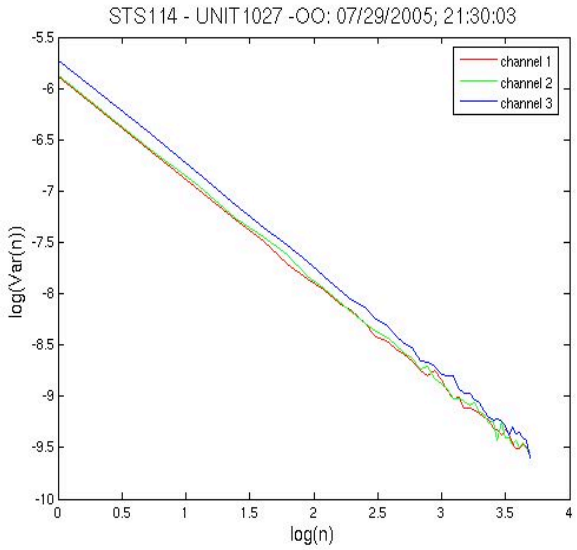

(b) Noise test

Fig. 13 Typical on-orbit white noise background as seen on unit 1027

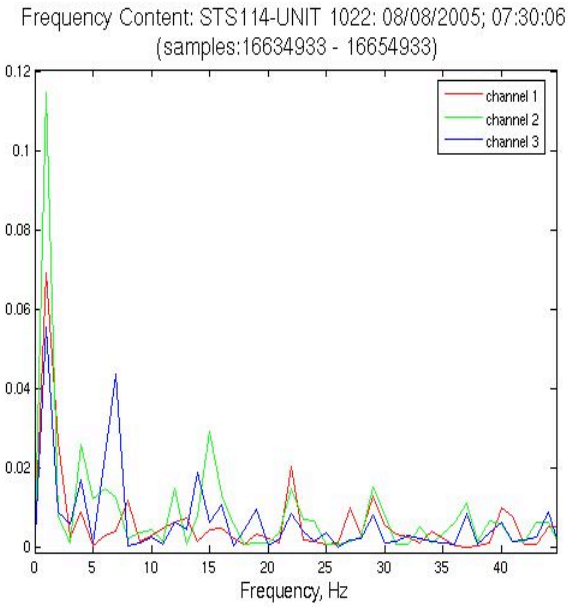

(a) Power spectrum

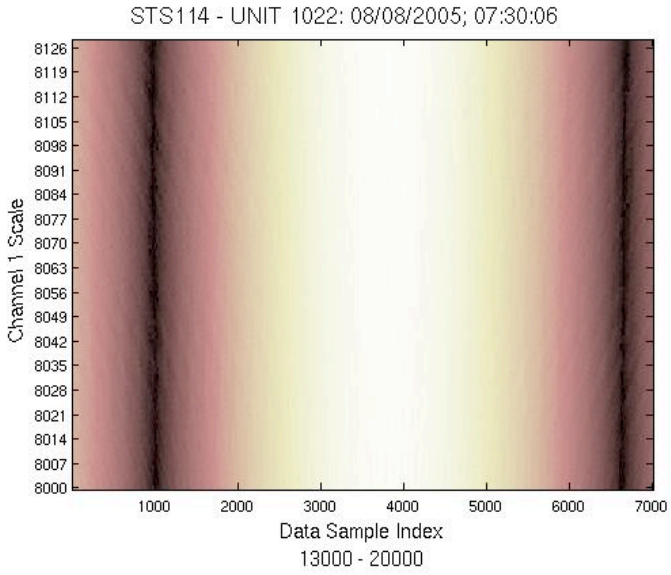

(b) Wavelet – channel 1

Fig. 14 A 1-2 Hz activity against on-orbit white noise background as seen on unit 1022

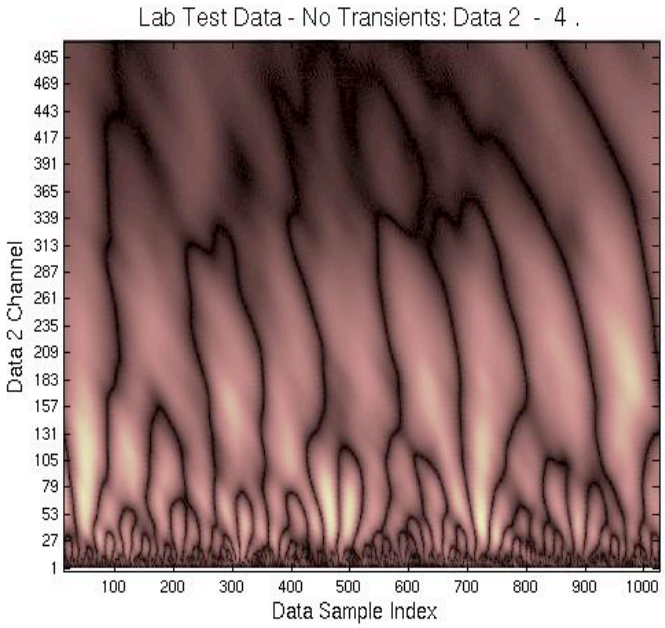

(a) Wavelet – Data 2

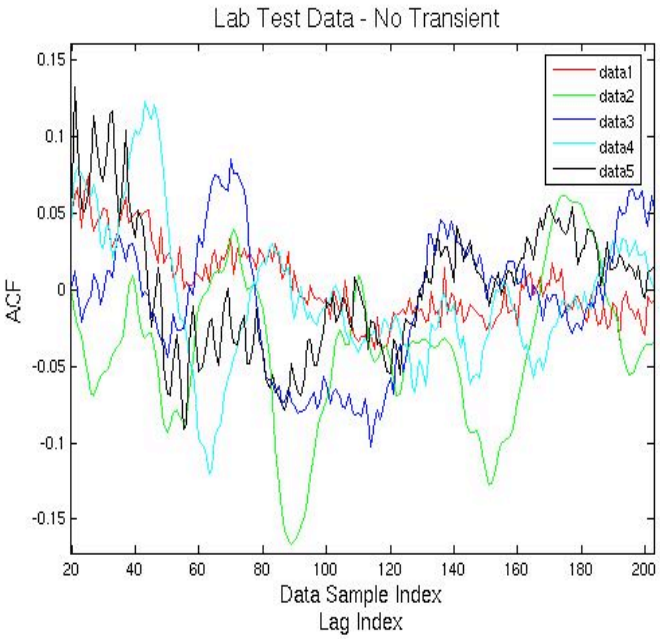

(b) Autocorrelation function

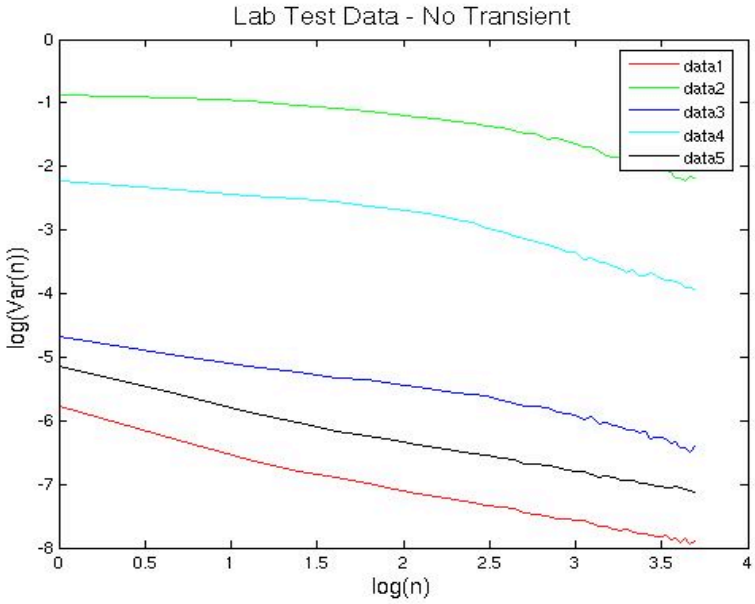

© Noise test

Fig. 15 Analysis of RespClass data shows strong self-similarity